

Optomechanical properties of a particle-waveguide system

A. V. Maslov*

University of Nizhny Novgorod, Nizhny Novgorod, Russia

(Received 12 March 2014; published 17 September 2014)

The balances of the electromagnetic powers and momentum flows for the system of a dielectric particle and a dielectric slab waveguide are studied. The emphasis is made on the regime when whispering gallery resonances in the particle are excited. The excitation is achieved by a guided mode that has either transverse electric or magnetic polarization. The scattering problem is solved by using an analytical representation of the solution with subsequent numerical approach to find the scattered fields with high accuracy. It accounts rigorously for the interaction between the particle and the waveguide. It is found that the propelling force on the particle can be comparable to or even exceed the value of the momentum flow of the incident mode. This is related to a highly anisotropic angular distribution of the bulk radiation that can carry some noticeable momentum in the longitudinal direction. The bulk radiation carries also nonvanishing momentum in the transverse direction giving rise to a difference in the transverse forces experienced by the particle and by the waveguide. The strong coupling between the particle and the waveguide operating in the single-mode regime is shown to upshift slightly the resonant frequencies with decreasing gap between the particle and the waveguide.

DOI: [10.1103/PhysRevA.90.033825](https://doi.org/10.1103/PhysRevA.90.033825)

PACS number(s): 42.50.Wk, 42.60.Da, 42.25.Fx

I. INTRODUCTION

The appearance of electromagnetic pressure associated with the electromagnetic fields is one of the key results of the Maxwell theory [1]. Due to the smallness of the electromagnetic forces that create the pressure, their effect can be seen most easily either on very large scales (for example, galaxy formation) or on very small scales. While the existence of forces were confirmed experimentally as far back as 1901 [2], their applications started to emerge much later, after the invention of laser [3].

Considering the forces on small dielectric objects, there are several research directions that are of current interest. One direction is designing new photonic devices in which the operation is related to the optical force acting on their components [4]. A typical example is the force created by a mode supported by two parallel waveguides [5,6]. This force can be significantly enhanced when the waveguide is coupled to a resonator [7–9] and used for tuning the optical transmission [10]. This enhancement goes together with narrow spectral linewidth of resonators such as microring filters [11]. Another direction is the manipulation of dielectric particles with optical fields, in particular with applications for the “lab-on-chip” approach for chemical and biological analysis [12]. The optical fields can be created either by optical beams in uniform medium (including free space) [13] or by evanescent fields of attenuated-total-reflection prisms or waveguides [14–17]. The force acting on a particle can also be enhanced by coupling the waveguide to a whispering-gallery-mode (WGM) [18], ring [19], or photonic-crystal-defect [20] resonator. Optical forces can be used for selective particle sorting as required by microsphere resonator circuits [21]. Recently, it was experimentally demonstrated that the modes of a tapered optical fiber can create large resonant forces on polystyrene spheres supporting WGMs [22]. The force created on the WGM particle was estimated to be comparable to

the flow of the electromagnetic momentum of the incident mode [23,24] or even exceed it [25]. Strong resonant pulling force acting on WGM particles can also be obtained using the excitation with backward waves [26].

Focusing specifically on applications that use waveguides, photonic devices rely on the transverse force which, unlike the longitudinal one, can bend the suspended portion of a waveguide and enable the control of the optical coupling and modal transmission [7,8]. On the other hand, the experiments on particle propulsion rely on both the longitudinal (propelling) force that moves the particle along the waveguide as well as on the transverse (trapping) force that holds the particle near the waveguide. There is a fundamental difference between these forces. The propelling force is created by the momentum flow of the initial guided mode. A finite value of the momentum flow puts a limit on the propelling force. The transverse force, on the other hand, is not limited by the incident momentum. This allows a significant build-up of the transverse force, especially using resonators.

Because of the interest in the optical propulsion technology, there is a need to look at the same time on both the longitudinal (propelling) and transverse (trapping) forces in the configuration that can be relevant to the experimental situations. In Ref. [23], the interaction of a dielectric particle with a surface wave supported by a metal boundary was studied. Here, a similar approach is extended to study a more realistic case in which the particle is excited using a dielectric slab waveguide. Both polarizations of the incident mode (transverse electric and magnetic) are considered. A comparison of the forces on the particle when it is excited by a plane wave and by a guided mode is made.

While the system of a resonator and a slab is different and geometrically simpler than that consisting of a microparticle and a tapered fiber used in the experiments [22], the two systems share an important ingredient—the presence of a strong coupling between their parts. This should give rise to similar qualitative features of the momentum flow and related propelling forces. The transverse force, on the other hand, may depend more strongly on the geometry of the

*avmaslov@yandex.ru

interaction region. Furthermore, the resonator-slab system allows one to obtain a very accurate solution without any further approximations such as neglecting the interaction between the waveguide and the particle which is often used in three-dimensional geometry [27].

The study of the interaction of a resonator with a slab is not a new problem. In fact, a large number of papers were devoted to understanding the properties of the system as well as to develop rigorous mathematical approaches to tackle it. This includes the use of integral method [28–30], finite-difference time-domain [31], and finite element in the frequency domain [32] approaches. However, the focus of the previous studies were only on such properties as transmission and reflection of guided modes. The balances of the electromagnetic flows in such systems, the properties of the propelling force, and the relation between the force and the momentum flows have not been considered. From this point of view, the present study of both the electromagnetic and optomechanical properties sheds more light on the physical processes in the system. In particular, it is found that the longitudinal force on the particle can be comparable or even exceed the value of the momentum flow of the incident mode. This is related to a highly anisotropic angular distribution of the bulk radiation that can carry some noticeable momentum in the longitudinal direction. The bulk radiation is also shown to carry nonvanishing momentum in the transverse direction. This momentum should give rise to a difference in the transverse forces experienced by the particle and by the waveguide. The strong coupling between the particle and the waveguide operating in a single-mode regime is also shown to give rise to a small frequency upshift with decreasing gap between the particle and the waveguide.

The paper is organized as follows. Section II specifies the physical model. Section III introduces basic equations, and describes the solutions of the scattering problem and calculation of forces. Section IV presents the properties for each component of the system (scattering properties for a particle in free space and the dispersion properties of a slab waveguide) and for the whole system (the excitation of the particle by a guided mode). Section V gives our conclusion.

II. FORMULATION OF THE PROBLEM

The studied physical model is illustrated in Fig. 1. We consider a dielectric particle (cylinder) that scatters a guided mode of the dielectric slab. The scattering particle is characterized by its radius R and dielectric constant ϵ_s . The particle is surrounded by a background with dielectric constant ϵ_b . The slab has thickness L and dielectric constant ϵ_g . The distance (gap) between the slab and the particle is d . The initial guided mode has power P_0 and frequency ω . As a result of the scattering, transmitted and reflected guided modes are created. Only the case when the waveguide supports one mode at the given ω , i.e., single-mode regime, will be explored. The scattering also produces bulk radiation that carries power P_b^+ in the upper and P_b^- in the lower half-spaces. The result of the scattering is the creation of the optical force \mathbf{F} that acts on the particle. Our aim is the analysis of the scattered radiation, the balances of the electromagnetic powers and momentum flows, and the properties of the created force.

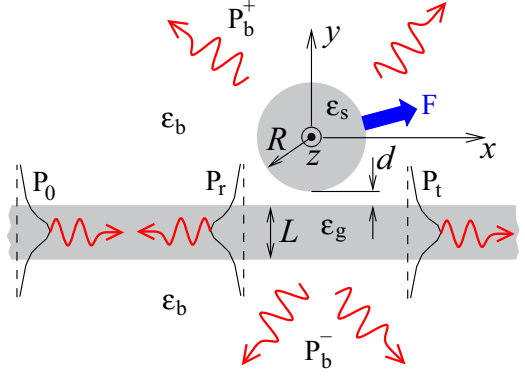


FIG. 1. (Color online) Geometry of the problem: a particle scatters an incident guided mode supported by the slab.

We consider only the two-dimensional geometry shown in Fig. 1. Within this geometry, two possible polarizations are studied. The first case is when the electric field of the incident mode has only z component [transverse electric (TE)]. The second case is when the magnetic field of the incident mode has only z component [transverse magnetic (TM)]. For all situations studied in this paper, the particle and waveguide are made of the same material with $\sqrt{\epsilon_s} = \sqrt{\epsilon_g} = 1.4$. The background is free space with $\epsilon_b = 1$.

III. SOLUTION OF THE PROBLEM

To find the force, we first solve for the field distribution created by scattering. After that, we calculate the force based on the Lorentz formula and show that it is consistent with that from the conservation of the flow of the electromagnetic momentum. We treat explicitly the TM case. This allows us to keep the notation simple and to refer to [23], which also considers the TM case. The TE case can be obtained with a rather straightforward modification of the formulas and, therefore, only results are given.

A. Finding the electromagnetic fields

We assume a $\sim e^{-i\omega t}$ dependence for all complex fields. The magnetic field of the incident TM mode (propagating in the $+x$ direction) has the following form for $y > -a$ ($a = R + d$):

$$H_z^i(x, y > -a) = B_0 e^{ih_0 x - \kappa_0(y+a)}, \quad (1)$$

where H_0 is the value of the magnetic field at $y = -a$ boundary. The wave number h_0 and the decay constant κ_0 are defined by the dispersion properties of the guided modes described in Sec. IV B.

The total field inside the particle is represented in terms of the cylindrical functions:

$$H_z(\mathbf{r}) = \sum_n A_n J_n(k_s r) e^{in\varphi}, \quad r < R, \quad (2)$$

where A_n are some unknown complex coefficients and $k_s = \sqrt{\epsilon_s} \omega / c$. The total field outside of the particle can be represented as a sum of the initial field (1) and scattered field:

$$H_z(\mathbf{r}) = H_z^i(\mathbf{r}) + H_z^s(\mathbf{r}). \quad (3)$$

The scattered field can be represented as a field created by some effective magnetic current $j(\varphi)$ localized on the particle surface:

$$H_z^s(\mathbf{r}) = \int_0^{2\pi} d\varphi' j(\varphi') G(\mathbf{r}, \mathbf{r}'), \quad (4)$$

where $G(\mathbf{r}, \mathbf{r}')$ is the Green's function for the system consisting of the background material and the slab. To adopt the approach of Ref. [23], we need to change the reflection coefficient in the integral representation of the Green's function. The reflection and transmission coefficients for a TM plane wave (with h being the x component of its wave number) incident on the slab are

$$r_{bg} = (1 - \xi^2) e^{i\phi_g} (e^{i\phi_g} - e^{-i\phi_g}) \mathcal{D}^{-1}, \quad (5a)$$

$$t_{bg} = 4\xi e^{i\phi_g} \mathcal{D}^{-1}, \quad (5b)$$

where

$$\mathcal{D} = (1 + \xi)^2 - (1 - \xi)^2 e^{2i\phi_g},$$

and $\xi = g_b \varepsilon_g / (g_g \varepsilon_b)$, $\phi_g = g_g L$, and $g_{g,b} = \sqrt{\varepsilon_{g,b} \omega^2 / c^2 - h^2}$. Replacing Eq. (19) of Ref. [23] with Eq. (5a) gives the required $G(\mathbf{r}, \mathbf{r}')$. The rest of the solution procedure remains the same. Similar to Eq. (2), we can expand the effective currents into angular components

$$j(\varphi) = \sum_{n=-\infty}^{\infty} j_n e^{in\varphi}. \quad (6)$$

Matching the tangential components of the fields inside and outside of the particle, we obtain a system of linear equations, which solving gives the expansion coefficients A_n and j_n . These coefficients allow us to find all scattered fields, both guided by the slab and propagating in the bulk medium. In particular, the distribution of the far-field radiation is needed for finding the balances of power and of momentum flow. The magnetic field in the far-field region is

$$H_z(\mathbf{r}) = \frac{f(\varphi)}{\sqrt{k_b r}} e^{-i\pi/4 + k_b r}. \quad (7)$$

The far-field distribution $f(\varphi)$ in Eq. (7) is

$$f(\varphi) = i \sqrt{\frac{\pi}{2}} \sum_n j_n (-i)^n J_n(k_b R) \times \begin{cases} [e^{in\varphi} + r_{bg}(k_{bx}) e^{-in\varphi + 2ik_{by}a}], & 0 < \varphi < \pi, \\ e^{in\varphi - ik_{by}L} t_{bg}(k_{bx}), & \pi < \varphi < 2\pi, \end{cases} \quad (8)$$

where $k_{bx} = k_b \cos \varphi$, $k_{by} = k_b \sin \varphi$, and $k_b = \sqrt{\varepsilon_b} \omega / c$. The reflection r_{bg} and transmission t_{bg} coefficients are given by Eq. (5).

B. Finding the electromagnetic force

There are three convenient ways to find the electromagnetic force acting on the particle using the known field distribution. We start with applying the Lorentz formula for the force acting on a dielectric object. The Lorentz force \mathbf{F} consists of two terms

$$\mathbf{F} = \mathbf{F}^e + \mathbf{F}^m, \quad (9)$$

where

$$\mathbf{F}^e = \int d\ell \sigma \mathbf{E}_\sigma, \quad \mathbf{F}^m = \frac{1}{c} \iint dS \frac{\partial \mathbf{P}}{\partial t} \times \mathbf{B}. \quad (10)$$

The first term \mathbf{F}^e describes the sum of all forces acting on small surface polarization charges $\sigma d\ell$ due to the presence of the field \mathbf{E}_σ created by other sources. The surface charge density σ is related to the jump of the bulk polarization \mathbf{P} . The polarization \mathbf{P} is obtained from the electric field and permittivity. In calculating \mathbf{E}_σ , the fields on both sides of the surface can be used to exclude the field created by the charge itself. The second term \mathbf{F}^m describes the force acting on the bulk current created by the oscillating polarization \mathbf{P} . The electric component of the force appears only on the surface of the particle, while the magnetic component is distributed over the volume.

For TM polarization, all quantities entering into Eq. (10) can be expressed using the expansion of the magnetic field (2) inside the particle. This allows one to integrate the Bessel functions and obtain the following expression for the x component of the Lorentz force (for $\varepsilon_b = 1$):

$$F_x^e = \frac{(\varepsilon_s - 1) c}{2\varepsilon_s^{3/2} \omega} \sum_n \text{Re}(A_n A_{n+1}^*) \left[(n+1) J_{n+1}^2(s) + n J_n^2(s) + \frac{\varepsilon_s - 1}{s} n(n+1) J_n(s) J_{n+1}(s) \right], \quad (11)$$

$$F_x^m = -\frac{\varepsilon_s - 1}{2\varepsilon_s^{3/2}} \frac{c}{\omega} s \sum_n \text{Re}(A_n A_{n+1}^*) J_n(s) J_{n+1}(s), \quad (12)$$

where $s = k_s R$. $\text{Re}(\xi)$ denotes the real part of a complex number ξ . The y components of the force can be calculated by taking the imaginary parts instead of the real parts in Eqs. (11) and (12). Note that the coefficients A_n represent the expansion of the total field inside the particle. According to (11) and (12), the existence of force requires the presence of at least two nonzero coefficients A_n . Expressions (11) and (12) allow one to calculate the force without any time-consuming integration procedures since all integrations were carried out analytically using the cylindrical functions.

Another approach to find the force is to use the Maxwell stress tensor. While the application of the Lorentz formula requires integration over the volume of the particle, the Maxwell stress tensor requires only integration over the surface outside the particle. Expressing the propelling force F_x for TM polarization using the Maxwell stress tensor one obtains

$$F_x = \frac{R}{8\pi} \int_0^{2\pi} d\varphi [(E_\rho^2 - E_\varphi^2 - H_z^2) \cos \varphi - 2E_\rho E_\varphi \sin \varphi], \quad (13)$$

where all fields are real and evaluated just outside the particle. It is convenient to express the fields outside the particle through the fields inside it using the usual boundary conditions. Using the expansion of the internal fields and integrating over the angle one arrives at exactly the same formula as the total force given by the sum of (11) and (12). As expected, the Lorentz formula and Maxwell stress tensor give the same result for the force in terms of the expansion coefficients for the fields inside. Using (13) gives the total force, rather than its electric

and magnetic components separately; see Eqs. (9) and (10). The components can still be separated even using the Maxwell stress tensor if one also integrates the tensor over the surface just inside the particle and uses the result to extract the force acting on the surface. Indeed, the electric component of the propelling force F_x^e in Eq. (10) can be written as

$$F_x^e = \frac{(\varepsilon_s - 1)R}{8\pi} \int_0^{2\pi} d\varphi [(\varepsilon_s + 1)E_\rho^2 \cos \varphi - 2E_\rho E_\varphi \sin \varphi], \quad (14)$$

where the fields are real and evaluated inside the particle. The same expression is obtained by taking the difference in (13) evaluated outside the particle and inside it and then expressing the fields outside in terms of the fields inside.

For TE polarization, the electric component of force in (9) is absent since there are no surface charges. The magnetic component of force is given by the same formula (12) as for the TM case except that A_n are the coefficients that describe the electric field E_z and there is an additional multiplier equal to $-\varepsilon_s$.

The force acting on the particle-waveguide system can also be found by considering the change of the flow of the electromagnetic momentum created by the incident mode and all scattered modes. The incident guided mode with wave number h_0 and power P_0 creates the momentum flow M_0 which is equal to

$$M_0 = \frac{h_0}{\omega} P_0. \quad (15)$$

The same formula can be used to find the momentum flow of the reflected and transmitted guided modes. For scattered bulk radiation, the momentum flow can be calculated by using its far-field distribution $f(\varphi)$. We also mention that the force in a multiport system can be calculated by finding variations in the transmission and reflection coefficients under some small displacement [33].

IV. RESULTS

Before considering the interaction between a particle and a waveguide, we study their individual properties. First, we start by considering the scattering of a plane wave on the particle. This allows us to identify the resonant modes of the particle and their spectral signatures. We study two quantities—the scattering cross section and the propelling force. Second, we study the waveguiding properties of the slab. And finally, we move to the scattering of the guided mode by the particle. This allows us not only to obtain the properties of the particle-waveguide system but also to identify its distinguishing features.

A. Free-space scattering

The problem of scattering of a plane wave by a particle in free space can be solved by expanding the fields inside and outside as well as the incident plane wave in terms of Bessel functions and applying the boundary conditions. The scattering cross section is then obtained by either calculating the power in the far-field region or by taking the scattering amplitude in the forward direction.

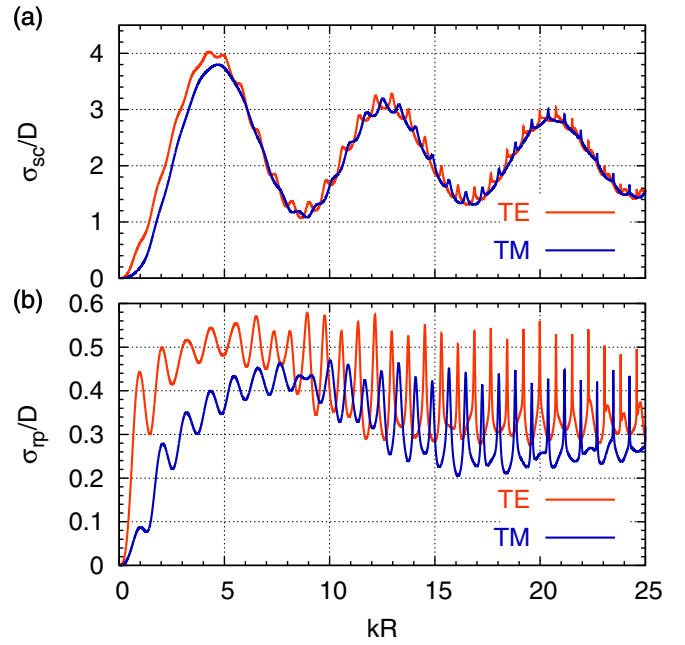


FIG. 2. (Color online) (a) Scattering σ_{sc}/D and (b) radiation pressure σ_{rp}/D cross sections as functions of kR for a plane wave with TE or TM polarizations incident on a scattering particle with $\sqrt{\varepsilon_s} = 1.4$ in free space $\sqrt{\varepsilon_b} = 1$.

The force can be calculated by substituting the expansion for the fields inside the particle into the Lorentz formula (11),(12). It is convenient to normalize the force to the power of the plane wave P_0 incident on the geometrical cross section equal to its diameter $D = 2R$. Alternatively, one can calculate the force from the momentum flow and express it in terms of the cross section for radiation pressure σ_{rp} [13]:

$$\frac{cF_x}{P_0} = \frac{\sigma_{rp}}{D}. \quad (16)$$

The cross section for radiation pressure is related to the extinction σ_{ext} and scattering σ_{sc} cross sections and to the far-field distribution $f(\varphi)$:

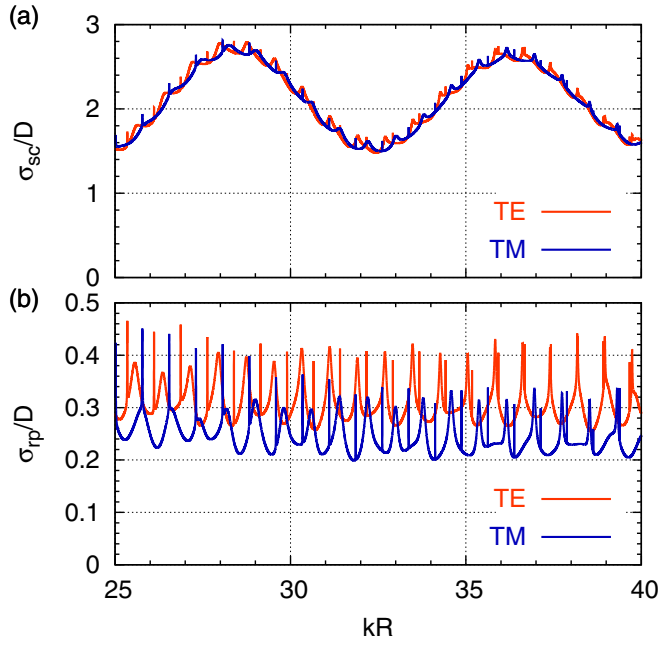
$$\sigma_{rp} = \sigma_{ext} - \langle \cos \varphi \rangle \sigma_{sc}, \quad (17)$$

where

$$\langle \cos \varphi \rangle = \frac{\int d\varphi \cos \varphi |f(\varphi)|^2}{\int d\varphi |f(\varphi)|^2}. \quad (18)$$

We calculated the left-hand side of (16) using the Lorentz formula and the right-hand side using the far field and obtained a perfect agreement.

The scattering and radiation pressure cross sections are shown in Figs. 2 and 3. The cross sections are plotted as functions of the dimensionless parameter kR with $k = \omega/c$. The scattering cross section shows a slow modulation with series of small and narrow peaks. These peaks correspond to the excitation of various order resonances. The most narrow peaks correspond to the excitation of WGMs. We refer as WGMs only to the modes with the lowest radial number. A remarkable feature is that the excitation of WGMs is much

FIG. 3. (Color online) Same as Fig. 2 but for larger kR .

more pronounced in the radiation pressure (or optical force) spectrum as compared to that in the scattering spectrum. However, the peaks of forces related to WGMs still remain comparable to the background level. The difference between TE and TM polarizations is mostly in the shift of the WGM resonances.

To understand the increased efficiency of the WGM excitation by guided modes later, let us look at the phase velocities of the WGMs. The phase velocity $v_{\text{ph}} = c/n_{\text{ph}}$ at the surface of the resonator is determined by its phase index

$$n_{\text{ph}} = \frac{nc}{\omega R}, \quad (19)$$

where ω is the frequency of the corresponding mode with azimuthal number n . The phase index for a WGM is found from the position of the corresponding scattering peak and its n . Another important property is the quality (Q) factor for the resonances that can be found by dividing the position of the peak to its FWHM (full width at half maximum). The phase index and the Q factor as functions of kR are plotted in Fig. 4. The phase index grows monotonically with increasing azimuthal number n or the parameter kR . The index for the TE modes is slightly greater than for the TM modes at similar values of n or kR . The phase index is between the values of the refractive indices of the background ($\sqrt{\epsilon_b} = 1$) and the particle ($\sqrt{\epsilon_s} = 1.4$). This is explained by the partial localization of energy inside and outside of the particle. The modes with $n < 15$ have rather small Q factors and are not shown in Fig. 4. On the other end, for $n > 55$, the Q factor becomes very large. The numerically calculated Q factors in Fig. 4(b) are fitted quite well with $\log_{10} Q \approx -0.481 + 0.145kR$ for TM polarization and $\log_{10} Q \approx -0.269 + 0.146kR$ for TE polarization. In practice, Q factors for the modes with large n will be limited by various absorption or scattering mechanisms that are not included in the considered model.

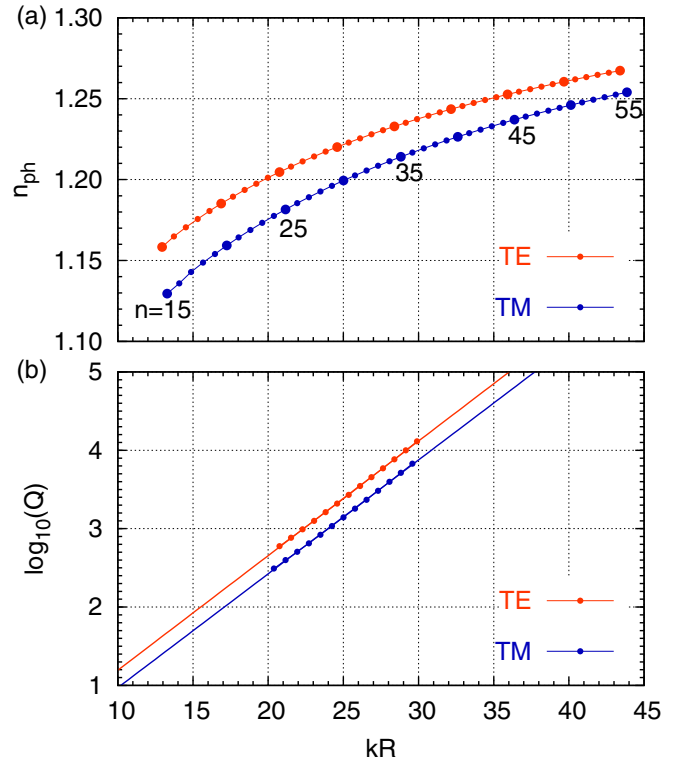


FIG. 4. (Color online) (a) Phase index for WGMs with azimuthal numbers $15 \leq n \leq 55$ for a particle with $\sqrt{\epsilon_s} = 1.4$. The dots show the calculated values for each mode and the line is a guide to the eyes. The larger dots show the modes with indices which are multiples of five. (b) Q factors for the WGMs. The dots show the calculated values and the straight lines are linear fits that extrapolate Q factors to the values of kR outside of the fitted range.

B. Dispersion for a slab waveguide

We now turn to the waveguiding properties of the slab. Figure 5 shows the phase index (ratio of the propagation wave number h and free-space wave number $k = \omega/c$) for the guided

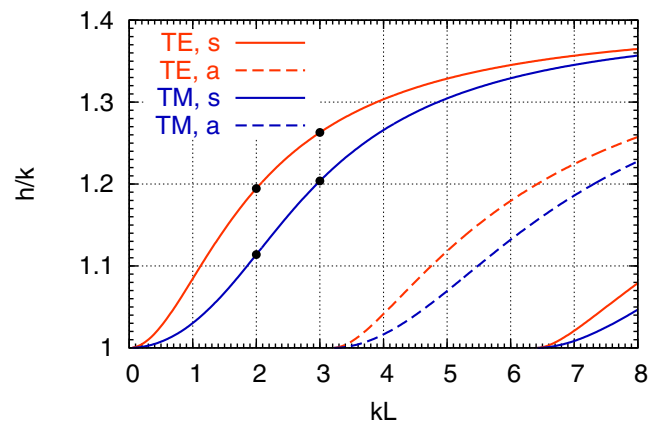


FIG. 5. (Color online) Dispersion for a slab waveguide with $\sqrt{\epsilon_g} = 1.4$. The modes are labeled according to their polarization (TE, TM) and symmetry of the transverse component of the field (s: symmetric; a: antisymmetric). The black dots show the operating points used for Figs. 6 and 8.

modes. The phase index lies between the refractive indices of the free space and the material of the slab. In order to operate in the single-mode regime, we choose kL below the cutoffs of the second (antisymmetric) modes for each type of polarization. For the slab, the cutoff conditions (same for TE and TM polarizations) are

$$kL = (m - 1)\pi/\sqrt{\varepsilon_g - \varepsilon_b}, \quad (20)$$

where $m = 1, 2, 3, \dots$ is the mode order. The single-mode condition becomes $kL < 3.2064$. We will investigate the cases of $kL = 3, 2$ (labeled by dots in Fig. 5). The phase indices for $kL = 3$ are $n_{\text{ph}} = 1.2629$ (TE) and $n_{\text{ph}} = 1.2037$ (TM). The phase indices for $kL = 2$ are $n_{\text{ph}} = 1.1946$ (TE) and $n_{\text{ph}} = 1.1139$ (TM).

C. Distribution of scattered powers

We now turn to the case when a guided mode propagates along the slab and is scattered by the particle. The scattering results in the creation of other guided modes and bulk radiation. Since we operate in the single-mode regime, there is only one transmitted and one reflected guided mode with powers P_t and P_r , respectively. The bulk radiation propagates in the half-spaces above and below the slab with powers P_b^+ and P_b^- , respectively. The power conservation states

$$P_t/P_0 + P_r/P_0 + P_b^+/P_0 + P_b^-/P_0 = 1 \quad (21)$$

and was verified numerically.

The dependences of the scattered powers on the dimensionless parameter kR are shown in Fig. 6. The transmission spectrum is characterized by a set of narrow dips that correspond to the pronounced peaks in the scattered bulk radiation. The reflected power remains very low. These features are related to the excitation of WGMs. In contrast to the scattering of a plane wave (shown in Figs. 2 and 3) no other resonances are clearly observable in the given range of kR . The excitation of WGM resonances shows maximum at around $kR \sim 25$. The decrease at larger kR can probably be attributed to the decrease of the phase index of WGMs [see Fig. 4(a)] and reduction of phase synchronization. However, the incident mode and the WGMs do not have to be synchronized accurately if the interaction between the particle and the waveguide is significant at small values of the gap kd . Note that the scattering characteristics shown in Figs. 6(a)–6(d) as functions of kR look quite similar for the two polarizations even though the incident TM mode has a lower phase index than that for the TE mode; see Fig. 5. However, the corresponding WGMs for TM polarization also have a lower phase index, see Fig. 4(a), and, therefore, the phase mismatch for both polarization is similar for a given kR . At resonances, the scattered powers in the upper and lower half-spaces have comparable values. At small kR , when the scattering does not have significant resonant enhancement, the scattering in the upper half-space is larger than in the lower half-space. Furthermore, the scattering of the TM wave is larger than the TE wave. This is most likely due to longer evanescent tails of the TM waves; see Fig. 5.

It is interesting to look at the distribution of the scattered bulk radiation. Figure 7 shows the far-field distributions at two values of kR : $kR = 24.597$ and $kR = 25.019$. All parameters are the same as for Fig. 6. At one value ($kR = 24.597$), the

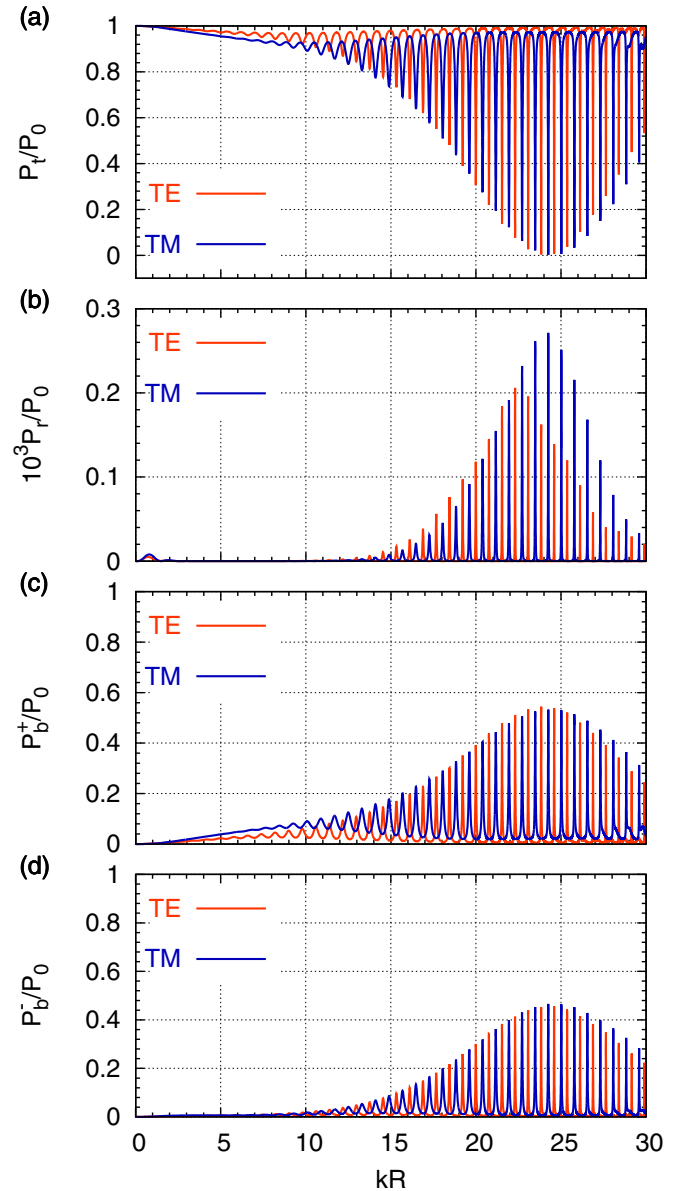


FIG. 6. (Color online) (a) Transmitted and (b) reflected powers of the guided mode and scattered bulk radiation in (c) upper and (d) lower half-spaces as functions of kR for $kd = 1.5$ and $kL = 3$.

resonant excitation of the TE mode takes place while the TM resonance is not excited. At the other value ($kR = 25.019$), the resonant excitation of the TM mode takes place while the TE resonance is not excited. These values of kR correspond to the excitation of the TE and TM WGMs with azimuthal number $n = 30$. The diagrams show normalized distributions but the scattered power at resonance is much larger than that at off resonance; see Fig. 6. Although the particle has a perfect circular shape, the scattered power has strongly anisotropic distribution. This can be explained by the fact that the scattering originates in the region where the particle is very close to the waveguide. The fast oscillations with angle (at $0 < \varphi < \pi$) arise from the interference of the fields emitted directly from the resonator and those that undergo reflection from the slab. Unlike the case of the initial surface wave guided

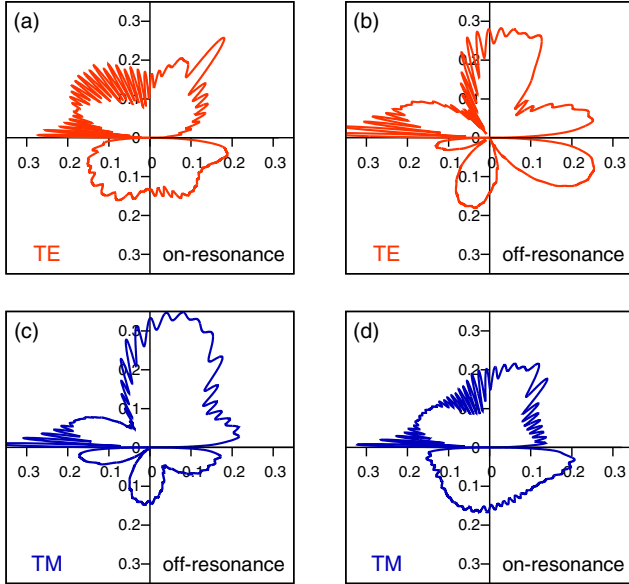


FIG. 7. (Color online) Angular distribution of power in the far-field region for (a),(c) $kR = 24.597$ and (b),(d) $kR = 25.019$. The other parameters are the same as for Fig. 6.

by a plasma boundary [23], the oscillations are not so deep due to only partial reflection of the waves from the slab.

D. Electromagnetic force

Let us now look at the forces acting on the particle. Figure 8 shows the forces that correspond to the situation shown in Fig. 6. In general, the dips in the transmission spectrum correspond directly to the resonant peaks of the propulsion force. The ratio cF_x/P_0 exceeds unity. Considering that the phase indices are $n_{\text{ph}} = 1.2629$ (TE) and $n_{\text{ph}} = 1.2037$ (TM), the force is comparable to $F_x \approx n_{\text{ph}}P_0/c$ for both polarizations. This means that the momentum flow of the initial wave is transformed into the propelling force on the resonator. The maximum value of force for the TE excitation is slightly larger than in the TM case, in agreement with the larger value of the phase index in the TE case. The smaller phase index for the TM case and, therefore, longer evanescent tail can also explain the slightly larger reduction in transmission for small kR for the TM polarization as compared to that for TE.

Let us now take a lower phase velocity of the initial wave by choosing a thinner slab $kL = 2$. The results are shown in Fig. 9. The thinner slab creates modes with longer evanescent tails outside of the slab. Therefore, it is natural that the transmission for small kR decreases faster than for $kL = 3$. The excitation of WGMs dominate the spectral features in this case as well. The minimum of transmission due to the excitation of WGMs moves to the region of smaller kR . This corresponds to the efficient excitation of WGMs with slightly lower phase indices, in agreement with the lower phase index of the incident mode.

The transverse force near the resonances has, in general, an asymmetric profile; see Figs. 8(c) and 9(c). In some cases, the peaks are almost antisymmetric, for example, the TM case shown in Fig. 8. In other cases, the peaks are clearly asymmetric. Moreover, the asymmetry can also have different shapes. For example, the asymmetry in the TE case in

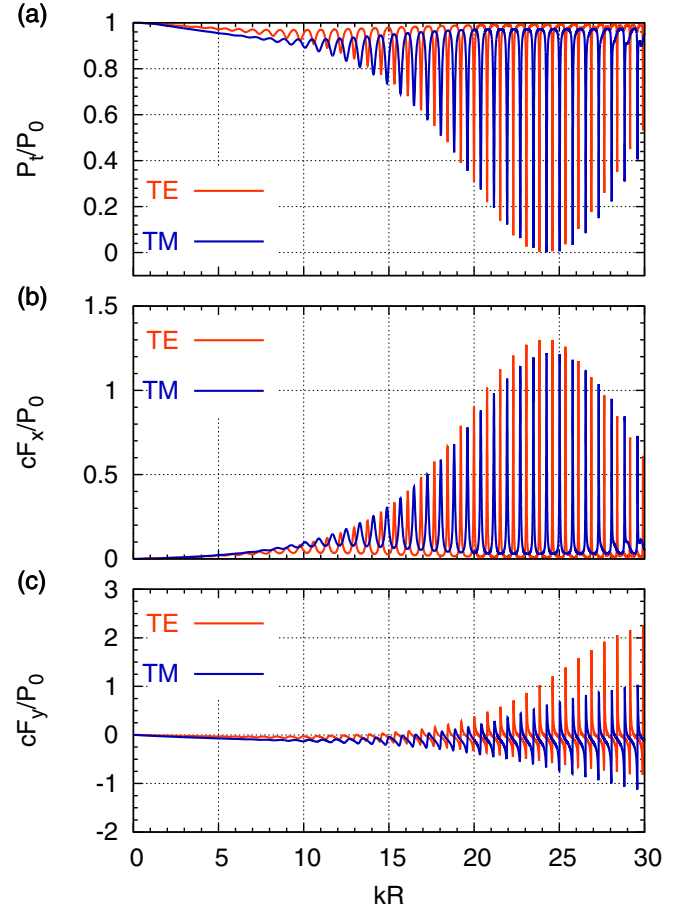


FIG. 8. (Color online) (a) Transmitted power, (b) longitudinal, and (c) transverse forces for the same parameters as Fig. 6. The transmission spectrum is replotted from Fig. 6 for convenience.

Fig. 8 is such that the positive high-energy side (repulsion) is significantly larger than the negative low-energy side (attraction) of the peak. For the TM case illustrated in Fig. 9(c) the opposite occurs: the positive high-energy side (repulsion) is significantly smaller than the negative low-energy side (attraction) of the peak. The asymmetry of the peaks can be explained using a phenomenological theory of resonator-waveguide coupling [8,34]. In that theory, the transverse force consists of two terms: antisymmetric and symmetric with respect to the resonant frequency. Depending on the coupling parameters, the sum of the two terms can produce various asymmetric shapes. The peaks of the transverse force can exceed that for the longitudinal force. This does not contradict the momentum balance.

Figure 9(b) shows that the maxima of the propelling forces can exceed slightly the momentum flow for the incident mode. This can only be explained by the noticeable momentum carried by the scattered bulk radiation. Figure 10 shows the momentum flow of the scattered bulk radiation along the x direction. While for small kR the momentum flow is positive, at resonances at $15 \lesssim kR \lesssim 30$, the momentum flow can become negative. This partial reflection explains the appearance of the propelling force that exceeds the momentum flow of the incident mode. It was verified that the force on the

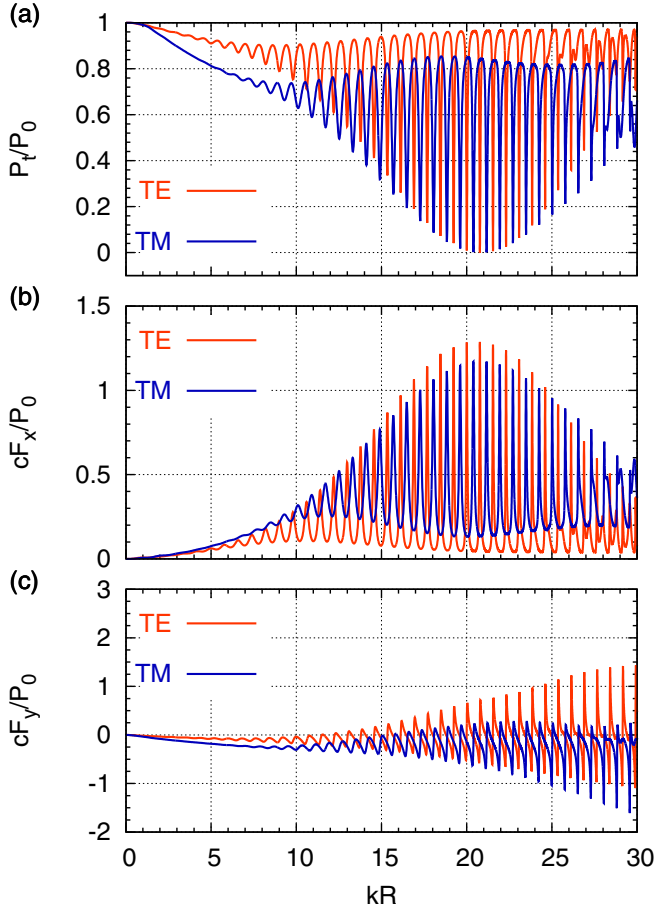


FIG. 9. (Color online) Same as Fig. 8 but for $kL = 2$.

resonator is equal to the difference in the momentum flow of the incident mode and all scattered fields (transmitted and reflected modes and bulk radiation). This means that the longitudinal force on the waveguide is zero.

The y component of the momentum flow of the bulk radiation is shown in Fig. 11. The upper and lower half-spaces create momentum flows in the opposite directions. However, the total momentum flow is not zero. This means that the transverse force on the particle is not equal to the transverse force on the waveguide. The total momentum flow of the scattered bulk radiation has positive y component. This is related to a slightly large bulk power scattered in the upper

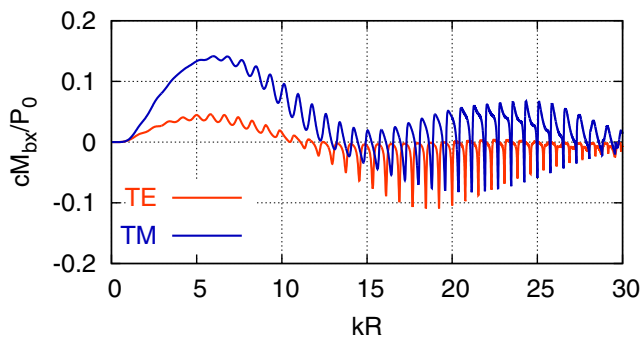


FIG. 10. (Color online) Momentum flow along the x direction of the scattered bulk radiation for the same parameters as Fig. 9.

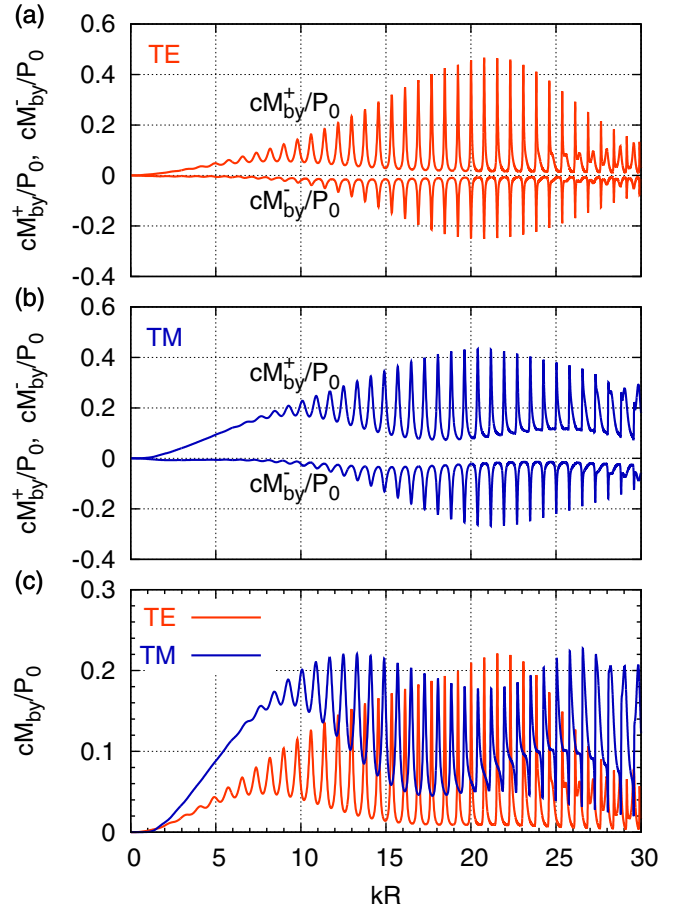


FIG. 11. (Color online) Momentum flow of the scattered bulk radiation along the y direction for the same parameters as Fig. 9. Frames (a) and (b) show the flows in the upper and lower half-space for each type of polarization. Frame (c) shows the total momentum flow.

half-space; see Figs. 6(c) and 6(d). Thus the total force on the particle and the waveguide should have a negative y component. The appearance of such a difference is a direct consequence of the scattering. This is in contrast to the interaction between two parallel waveguides where the transverse forces acting on the waveguides have opposite directions due to the absence of scattering.

E. Single resonant peak

We now focus on the properties of a single resonant peak and how they change with varying gap. In practice, such measurements are performed by scanning the wavelength, usually in a relatively narrow range. This leads to changes in kd and kR at the same time. In this particular situation, the convenient dimensionless parameters are d/R , L/R , and kR . However, to be somewhat more specific let us choose $R = 5 \mu\text{m}$, $L = 0.6 \mu\text{m}$ and look at the features related to the excitation of WGMs with $n = 30$ (see Figs. 12 and 13) by scanning the wavelength as several values of d . Starting from a large d , the minimum of transmission initially becomes lower, reaches zero, and then starts to increase. This is accompanied by a monotonic broadening of the peak. The peak of the

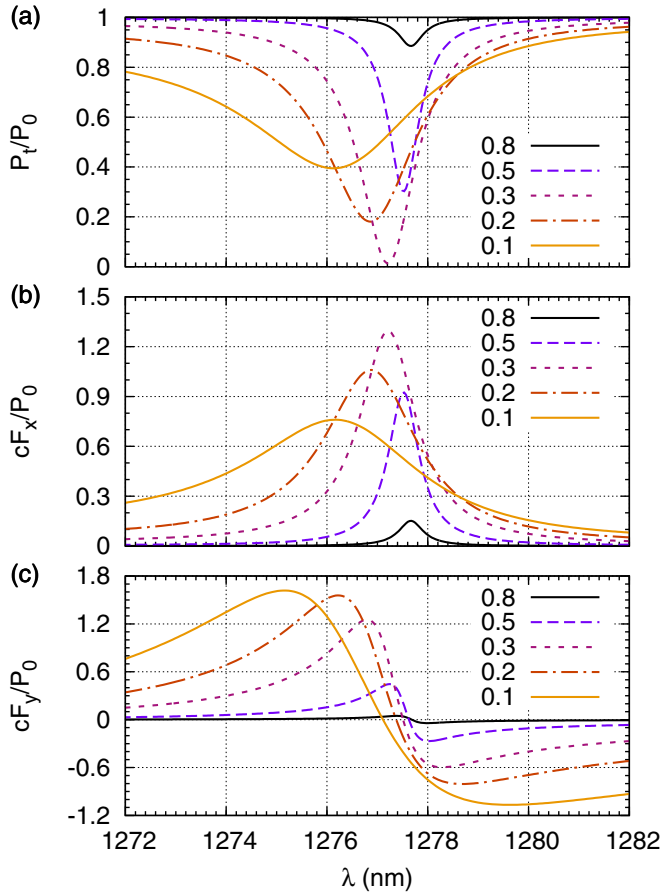


FIG. 12. (Color online) (a) Transmitted power, (b) longitudinal force, and (c) transverse force as functions of wavelength at several values of gap d (in μm , labeled for each curve) for $R = 5 \mu\text{m}$, $L = 0.6 \mu\text{m}$, and TE polarization.

longitudinal force correlates well with the dip in transmission. The transverse force has asymmetric features, as explained in Sec. IV D.

It is interesting that the decrease in the gap leads to the shift of the peak into the region of shorter wavelengths (blueshift). However, the higher index of the slab as compared to free space is expected to move it towards longer wavelengths. For example, the redshift is often attributed to the effective increase of the refractive index or the size of the resonator and it is a basis for highly sensitive detection of various molecules [35]. Furthermore, one also expects that broadening of the resonance due to the increased scattering should shift the resonance to longer wavelengths, according to the general property of a damped harmonic oscillator. The reason for such a counterintuitive behavior can be the strong interaction with the guided mode, in contrast to the perturbative approaches that predict a redshift. Indeed, a decrease in the gap makes the distance between the phase fronts created by the WGM at the waveguide location shorter due to the curvature of the resonator surface. The shorter distance between the phase fronts means that the synchronization occurs with a guided mode with a larger wave number, and thus a larger frequency. Thus the strong interaction should increase the frequency of the resonator coupled to the waveguide. Although the shifts are rather small in Figs. 12

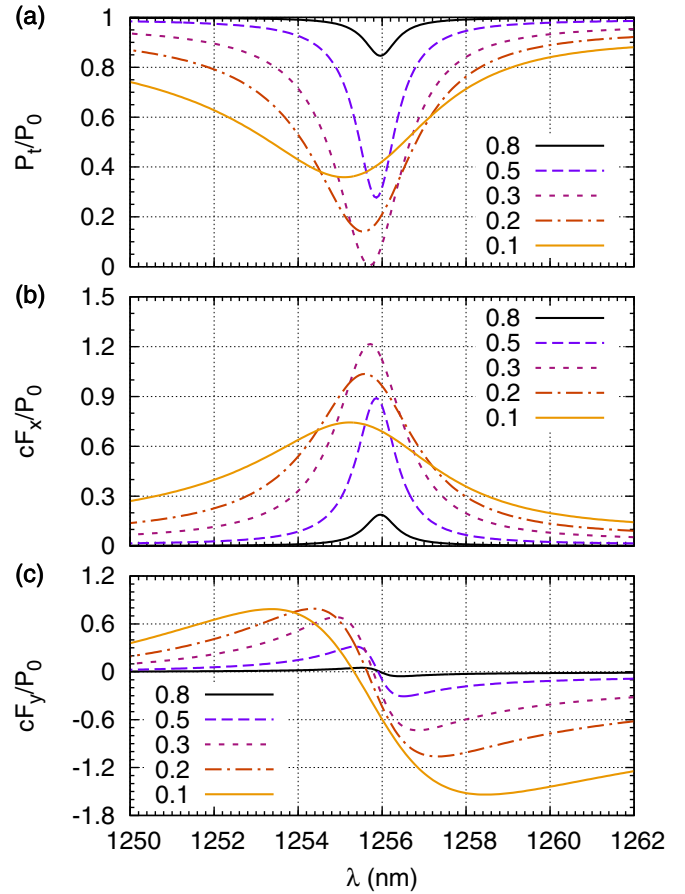


FIG. 13. (Color online) Same as Fig. 12 but for TM polarization.

and 13, much larger frequency upshifts were predicted when a WGM resonator is coupled to a surface plasmon [23].

We note that in Ref. [32] the simulations produced the shifts of the resonant mode downwards or upwards depending on the microcavity-waveguide configuration and the resonant mode. The frequency upshift was in the regime when the waveguide was only slightly above the cutoff condition for the second mode, while the downshifts were in multimode regimes. Our simulations with slabs operating in multimode regimes also resulted in frequency downshifts of the resonances. Apparently, the single-mode regime plays an important role in inducing the upshift of the resonant frequency of the resonator.

V. CONCLUSIONS

To conclude, a comprehensive analysis of the optomechanical properties of the system consisting of a particle coupled to a slab waveguide is presented. The results are obtained by a rigorous solution of the Maxwell equations and account fully for the interaction between the particle and the waveguide. The problem is assumed to be two dimensional and both polarizations (TE and TM) are investigated. It is shown that the efficient excitation of the WGMs in the particle by a guided mode gives rise to the creation of the propelling force on the particle with values comparable to or even exceeding the value of the momentum flow of the incident mode. This is explained by the presence of some longitudinal momentum

of the scattered bulk radiation in the backward direction. The bulk radiation has an anisotropic distribution in a wide angular range. The transverse momentum of the bulk radiation produces a difference in the magnitudes of the forces acting on the particle and on the waveguide. It was also shown that the frequencies of the WGMs in the particle can be slightly upshifted (blueshift) with decreasing particle-to-slab distance.

ACKNOWLEDGMENTS

This work was supported in part by the Ministry of Education and Science of the Russian Federation through Agreements No. 11.G34.31.0011 and No. 02.B.49.21.0003. The author acknowledges stimulating discussions with V. N. Astratov, Y. Li, and M. I. Bakunov.

-
- [1] J. C. Maxwell, *A Treatise on Electricity and Magnetism, Vol. II* (Macmillan and Co., London, 1873), pp. 391–392.
- [2] P. N. Lebedev, *Ann. Phys. (Leipzig)* **311**, 433 (1901).
- [3] A. Ashkin, *Proc. Natl. Acad. Sci. USA* **94**, 4853 (1997).
- [4] P. T. Rakich, M. A. Popović, M. Soljačić, and E. P. Ippen, *Nat. Photon.* **1**, 658 (2007).
- [5] M. Povinelli, M. Lončar, M. Ibanescu, E. Smythe, S. Johnson, F. Capasso, and J. Joannopoulos, *Opt. Lett.* **30**, 3042 (2005).
- [6] M. Li, W. H. P. Pernice, and H. X. Tang, *Nat. Photon.* **3**, 464 (2009).
- [7] M. Eichenfield, C. P. Michael, R. Perahia, and O. Painter, *Nat. Photon.* **1**, 416 (2007).
- [8] M. Li, W. H. P. Pernice, and H. X. Tang, *Phys. Rev. Lett.* **103**, 223901 (2009).
- [9] V. Intaraprasong and S. Fan, *Phys. Rev. A* **86**, 063833 (2012).
- [10] A. Einat and U. Levy, *Opt. Express* **19**, 20405 (2011).
- [11] B. E. Little, S. T. Chu, H. A. Haus, J. Foresi, and J.-P. Laine, *J. Lightw. Technol.* **15**, 998 (1997).
- [12] D. Erickson, X. Serey, Y.-F. Chenac, and S. Mandal, *Lab Chip* **11**, 995 (2011).
- [13] W. N. Irvine, *J. Opt. Soc. Am.* **55**, 16 (1965).
- [14] H. Y. Jaising and O. G. Hellesø, *Opt. Commun.* **246**, 373 (2005).
- [15] B. S. Schmidt, A. H. J. Yang, D. Erickson, and M. Lipson, *Opt. Express* **15**, 14322 (2007).
- [16] J. Ng and C. T. Chan, *Appl. Phys. Lett.* **92**, 251109 (2008).
- [17] J. J. Xiao, J. Ng, Z. F. Lin, and C. T. Chan, *Appl. Phys. Lett.* **94**, 011102 (2009).
- [18] S. Arnold, D. Keng, S. I. Shopova, S. Holler, W. Zurawsky, and F. Vollmer, *Opt. Express* **17**, 6230 (2009).
- [19] S. Lin, E. Schonbrun, and K. Crozier, *Nano Lett.* **10**, 2408 (2010).
- [20] A. Rahmani and P. C. Chaumet, *Opt. Express* **14**, 6353 (2006).
- [21] V. N. Astratov, in *Photonic Microresonator Research and Applications*, Springer Series in Optical Sciences Vol. 156, edited by I. Chremmos, O. Schwellb, and M. Uzunoglu (Springer, New York, 2010), Chap. 17, pp. 423–457.
- [22] Y. Li, O. V. Svitelskiy, A. V. Maslov, D. Carnegie, E. Rafailov, and V. N. Astratov, *Light: Sci. Appl.* **2**, e64 (2013).
- [23] A. V. Maslov, V. N. Astratov, and M. I. Bakunov, *Phys. Rev. A* **87**, 053848 (2013).
- [24] V. N. Astratov, Y. Li, O. V. Svitelskiy, A. V. Maslov, M. I. Bakunov, D. Carnegie, and E. Rafailov, *Opt. Photon. News* **24**, 40 (2013), special issue 12: Optics in 2013.
- [25] A. V. Maslov and M. I. Bakunov, *Opt. Lett.* **39**, 2823 (2014).
- [26] A. V. Maslov, *Phys. Rev. Lett.* **112**, 113903 (2014).
- [27] A. N. Oraevsky, *Quantum Electron.* **32**, 377 (2002).
- [28] V. I. Kalinichev and P. N. Vadov, *Radiotekh. Elektron.* **33**, 464 (1988) (in Russian).
- [29] A. I. Nosich, *IEEE Antennas Propag. Mag.* **41**, 34 (1999).
- [30] S. V. Boriskina and A. I. Nosich, *IEEE Trans. Microw. Theory Tech.* **47**, 224 (1999).
- [31] S. C. Hagness, D. Rafizadeh, S. T. Ho, and A. Taflove, *J. Lightw. Technol.* **15**, 2154 (1997).
- [32] Z. Guo, H. Quan, and S. Pau, *J. Phys. D: Appl. Phys.* **39**, 5133 (2006).
- [33] P. T. Rakich, M. A. Popović, and Z. Wang, *Opt. Express* **17**, 18116 (2009).
- [34] V. Intaraprasong and S. Fan, *Opt. Express* **21**, 25257 (2013).
- [35] F. Vollmer and S. Arnold, *Nat. Methods* **5**, 591 (2008).